Unusual Width Dependence of Lattice Thermal Conductivity in Ultra-Narrow Armchair Graphene Nanoribbons with Unpassivated Edges

Qi Wang [a], Ruiqiang Guo [b], Baoling Huang [c], Yue Chen [a,d] *

[a] *Department of Mechanical Engineering, The University of Hong Kong, Pokfulam Road, Hong Kong SAR, China*

[b] *Department of Mechanical Engineering and Materials Science, University of Pittsburgh, Pittsburgh, Pennsylvania 15261, USA*

[c] *Department of Mechanical and Aerospace Engineering, The Hong Kong University of Science and Technology, Clear Water Bay, Hong Kong SAR, China*

[d] *HKU Zhejiang Institute of Research and Innovation, 1623 Dayuan Road, Lin An 311305, China.*

Abstract

Low-dimensional materials attract extensive interest in electronic applications since the synthesis of graphene. Understanding the thermal transport in low-dimensional materials with shrinking characteristic size where strong confinement effect occurs is of importance for the thermal management

* Corresponding author. Tel: 852-39177095. E-mail: yuechen@hku.hk

of nano electronics. Recently, the atomically precise armchair graphene nanoribbons (AGNRs) with well-defined edges have been successfully synthesized. Serving as the fundamental functional elements, AGNRs can potentially make novel nano electronics realizable. Here we systematically investigate the thermal property variations of the ultra-narrow AGNRs with width without hydrogen termination using the density-functional-based tight binding (DFTB) method, which combines the accuracy of density functional theory and the efficiency of tight-binding approximation. The lattice thermal conductivity increases unexpectedly from 531.7 W/m-K to 3470.6 W/m-K as the width decreases from 0.97 to 0.35 nm, different from the width dependence in larger scales; the lattice constants, low frequency phonon group velocities and lifetimes, and acoustic phonon contributions also show increasing trends as the width decreases. Such behaviors are attributed to the changes in the lattice constants and the phonon scattering channels of the dominant low frequency acoustic phonons. Further DFTB calculations reveal that planar ultra-narrow armchair BN nanoribbons also show analogous trends in thermal properties with the shrinking width. This study unveils the width-dependent phonon transport behaviors of ultra-narrow planar nanoribbons and offers guidelines for the thermal design of potential nano electronics.

1. Introduction

Graphene-based low-dimensional materials have attracted extensive attention in recent years due to their exceptional mechanical,[1] electrical,[2] and thermal properties.[3] Graphene nanoribbon (GNR), the strip of graphene, is one of the most well-researched nanostructures among them. The adjustable width makes the physical properties of GNRs tunable for potential applications. For the electrical properties, the armchair GNRs (AGNRs) show increased band gaps as the width decreases[4-6] in the nanoscale regime, providing opportunities for atomically controlling features of gap-modulated semiconductor junctions.[7] For the mechanical property, the Young's modulus demonstrates a general increasing trend as the width increases.[8-10] For the magnetic properties, compared to the nonmagnetic 2D planar graphene,

zigzag GNRs (ZGNRs) have magnetic edges which can be modulated and the related properties are width-dependent.[11,12] GNRs are also 1D symmetry-protected topological materials characterized by the Z_2 invariant[13] and the topological properties are closely related to the width.[14,15] Thus, it is very fundamental yet essential to investigate the width dependence of the physical properties of GNRs for the multiple potential micro-nano devices.

As for the thermal properties, a few experiments have been conducted to investigate the size dependence of thermal transport in GNRs.[16-20] In general, AGNRs without hydrogen termination are less stable that the AGNRs with hydrogen termination. Due to the uncontrollable defects, edge roughness, polymeric residues of samples and the different measurement techniques,[20] high-quality single-crystal graphene and GNRs are difficult to be synthesized, suspended, and measured. The measured thermal conductivity of 2D graphene is still inconsistent,[21,22] and the measurements of thermal conductivity of GNRs in nanoscale is rare. Bae *et al.* measured the thermal conductivities of different substrate-supported GNR samples with widths of 45-130 nm (with considerable edge roughness) and found that the thermal conductivity scales with the width approximately as $\sim W^{1.8\pm0.3}$.[16] In fact, only a few experimental measurements of the thermal properties of GNRs have been done in the width range of tens of nanometer,[16,23,24] let alone for the ultra-narrow GNRs with well-defined edges. Recently, atomically precise AGNRs with well-defined edges (e.g., 7-AGNR, 9-AGNR and their heterostructures with hydrogen termination) have been realized by polymerization of dedicated molecular precursors.[14,15,25,26] Therefore, a full and accurate understanding of the thermal transport in these atomically precise GNRs is necessary.

Many theoretical efforts have been devoted to studying the thermal transport in GNRs with different widths. It is predicted that the thermal conductivity of ZGNRs is higher than that of AGNRs with the same width,[27-31] and the thermal conductivity of both types can be reduced by edge conditions (hydrogen

termination[32] and roughness[29,32-34]). Moreover, many theoretical studies based on empirical potentials tried to extract the width dependence of the thermal conductivity of GNRs in various size ranges at room temperature. Using the equilibrium molecular dynamics (MD) simulations with empirical potentials, several studies demonstrated that the thermal conductivity of smooth GNRs decreases as the width decreases in the size range from 40 to 1.7 nm,[27,33,35] agreeing well with the expectation that classical size effect suppresses phonon transport (The finite sample size introduces boundaries or edges as extra phonon scattering sources). However, based on the Boltzmann transport equation (BTE) method with the interatomic force constants (IFCs) calculated from an optimized Tersoff potential,[36] Lindsay *et al.* found that the thermal conductivity of AGNRs increases from $\kappa_{graphene}$ to $1.2 \cdot \kappa_{graphene}$ as the width decreases from 2.7 to 0.42 nm.[37] In their study, the width W ($W = \pi d$) of AGNR was fixed to the perimeter of a corresponding single-wall carbon nanotube (SWCNT). Because the lattice structures were not fully relaxed, it also led to a contradiction that all AGNRs have a thermal conductivity above or equal to that of graphene.[35]

The width dependence of thermal conductivity of the ultra-narrow AGNRs is still controversial because of the limitations in the accuracy and transferability of empirical potentials. For instance, it was reported that based on equilibrium MD simulations with Brenner potential,[38] 24.6 nm in length is large enough to eliminate the size effect for phonon transport in GNRs at room temperature;[30] whereas, an optimized Tersoff potential[36] yielded a minimal length range of 75 - 100 nm,[27] despite their different absolute values (467 W/m-K compared to 680 W/m-K for AGNR with a width of around 4 nm). These problems may be overcome by the BTE method with precise IFCs calculated from density functional theory (DFT), which has achieved great success in predicting phonon transport properties in various materials.[39-42] However, the DFT calculations for accurate IFCs demand a large computational cost and

can only be applied to simple crystals. Currently, for GNRs the DFT calculations for IFCs are very time-consuming.

The density-functional-based tight binding (DFTB) method, combining the accuracy of DFT calculations and the efficiency of the tight-binding method, can be a good quantum simulation choice for thermal property calculations of GNRs. With proper precalculated and tabulated DFTB parameters, this method can be two orders of magnitude faster than DFT calculations without losing much accuracy and has been used in studying the phonon transport in graphene,[43,44] MOF-74,[45] and Si-based materials,[46,47] demonstrating its good transferability. In this paper, we investigate the thermal transport properties of ultra-narrow AGNRs without hydrogen termination based on the DFTB calculations within the BTE scheme. Unlike ZGNRs, the calculations of AGNRs require no spin-polarization effects[48] and can be implemented more easily. The AGNRs without hydrogen termination eliminate the passivation effect on thermal transport, and they are also semiconducting[6] (also see Fig. S1, Supporting Information). The semiconducting nature means that the electronic contribution to thermal transport in the AGNRs without hydrogen termination may be ignored. We calculated the thermal conductivity of the N-AGNRs (N: 4-9) using the full iterative solution of BTE and found that the thermal conductivity increases largely as the width decreases from 0.97 to 0.35 nm. To better understand the width dependence, the detailed analysis of the lattice constants, phonon group velocity, lifetimes, and mean free paths (MFPs) of N-AGNRs is performed. For AGNRs with a narrower width, the dominant low frequency phonons in thermal transport exhibit lower scattering rates and larger phonon group velocities, which are demonstrated through the analysis of the elongation of lattice constants along the armchair direction and the weighted phase space of low frequency phonons. Similar behavior is also observed in armchair BN nanoribbons (ABNNRs) with respect to its width. The corresponding mechanism for the width dependence is discussed.

2. Method

According to Fourier's law and the kinetic theory, the lattice thermal conductivity can be expressed as a summation of contributions from all the phonon modes λ denoted by wavevector $\boldsymbol{q}$ and phonon polarization *s*,

$$\kappa_{\alpha\beta} = -\frac{1}{N_0 V}\sum_{\lambda}\hbar\omega_{\lambda}v_{\lambda}^{\alpha}f_{\lambda}^{0}(f_{\lambda}^{0}+1)F_{\lambda}^{\beta}, \tag{1.1}$$

where *α, β* are the Cartesian indices, N_0 is the total number of *q*-points in the first Brillouin zone, *V* is the unit cell volume, ω is the phonon frequency, $\boldsymbol{v}$ represents the phonon group velocity ($\boldsymbol{v}_{\lambda} = \partial\omega_{\lambda}/\partial\boldsymbol{q}$), and f_{λ}^{0} stands for the equilibrium phonon Bose-Einstein occupancy. $\boldsymbol{F}$ is the linear phonon perturbation vector, which is related to the real occupancy $f_{\lambda} = f_{\lambda}^{0} + f_{\lambda}^{0}(f_{\lambda}^{0}+1)\boldsymbol{F}_{\boldsymbol{\lambda}}\cdot\nabla T$, and can be calculated by iteratively solving the BTE,[49-51]

$$-v^{\alpha}(\lambda)f_{\lambda}^{0}\left(f_{\lambda}^{0}+1\right)\frac{\hbar\omega_{\lambda}}{k_B T^2} = \tilde{p}_{\lambda,\lambda'}F_{\lambda}^{\alpha}, \tag{1.2}$$

$$\tilde{p}_{\lambda\lambda'} = \frac{1}{2}\sum_{\lambda'',\lambda'''}\left(P_{\lambda,\lambda'''}^{-\lambda''} + P_{\lambda,\lambda''}^{-\lambda'''} + P_{\lambda''',\lambda''}^{-\lambda}\right)\delta_{\lambda\lambda'} + \sum_{\lambda''}\left(P_{\lambda,\lambda'}^{-\lambda''} + P_{\lambda,\lambda''}^{-\lambda'} + P_{\lambda',\lambda''}^{-\lambda}\right), \tag{1.3}$$

$$P_{\lambda,\lambda'}^{\lambda''} = 2\pi f_q^0 f_{q'}^0\left(f_{q''}^0+1\right)|V_3(\lambda,\lambda',\lambda'')|^2\delta(\omega_{\lambda}+\omega_{\lambda'}-\omega_{\lambda''}). \tag{1.4}$$

Here $\tilde{p}_{\lambda,\lambda'}$ is the combined scattering matrix, $P_{\lambda,\lambda'}^{\lambda''}$ is the three-phonon scattering probability. Three phonon scattering processes satisfy the energy conservation, $\omega_{\lambda} \pm \omega_{\lambda'} \pm \omega_{\lambda''} = 0$, and $P_{\lambda,\lambda'}^{\pm\lambda''}$ represents the three-phonon scattering probability for the process $\omega_{\lambda} + \omega_{\lambda'} \pm \omega_{\lambda''} = 0$. δ is the Dirac delta function, and V_3 is the third order force constant projected onto the eigenvector space.[52] Using the above equations with the second and third order IFCs as inputs, the lattice thermal conductivity can be calculated iteratively. In this study, all IFCs are calculated efficiently by the DFTB method via DFTB+[53] along with the selected parameters.[54,55] In the DFTB method, the total energy of a system is the second order

Taylor expansion of the Kohn-Sham total energy in DFT with respect to charge density fluctuation.[56-59] The DFTB parameters used in this study have been verified to give the accurate description of phonon transport properties including phonon dispersion relations, phonon lifetimes, and thermal conductivities of 2D graphene and BN.[43,44]

Since ultra-narrow AGNRs are quasi-1D structures, only the lattice constant (a) along the armchair direction (x direction as shown in Fig. 1) needs to be optimized. A vacuum layer with a thickness of at least 15 Å was used to avoid the interactions between adjacent nanoribbons in the other two directions. While optimizing the lattice constant a, the atoms in the unit cell were also allowed to move in all three directions. The total electronic energy tolerance was set to 10^{-8} eV for the DFTB calculations. All the AGNRs were optimized using DFTB+ with a 15×1×1 k-point sampling grid and a convergence criterion of 10^{-6} eV/Å for atomic forces. When calculating the second and third order IFCs of the N-AGNRs, a 9×1×1 supercell (2N×9 atoms) was used. A cutoff distance of at least 8 Å was adopted in calculating the third order IFCs to reduce computational cost without losing much accuracy. The lattice thermal conductivity was calculated on a 1100×1×1 $\boldsymbol{q}$ mesh to guarantee the convergence (see Supporting Information). In addition, the monolayer thicknesses of AGNRs and ABNNRs were taken as 3.35 and 3.31 Å, respectively, corresponding to the van der Waals diameters of the constituent atoms. The actual width of AGNRs is defined as the maximum distance along the y direction between the outmost edge atoms as shown in Fig. 1.

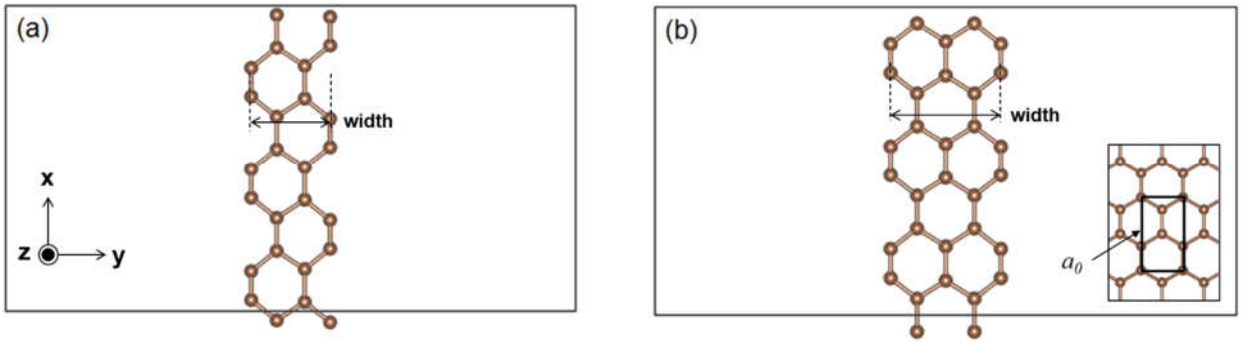

Fig. 1 The optimized structures of (a) 4-AGNR and (b) 5-AGNR. Supercell: 3×1×1. The inset indicates the unit cell (dark black box, 4 atoms) of graphene, and a_0 is the lattice parameter along the armchair direction.

3. Results and discussion

3.1. Structures and harmonic properties of AGNRs

After the DFTB relaxation, the edges of AGNRs are well-defined, and all the atoms are in the same *xy* plane. The optimized structures of 4-AGNR and 5-AGNR are shown in Fig.1 as representatives. The lattice constants and widths of AGNRs are listed in Table 1. Compared to the corresponding parameter of graphene a_0 = 4.316 Å (see the inset of Fig. 1), the lattice constants of AGNRs are slightly larger and show an ascending trend with decreasing width, which is consistent with previous first-principles calculations.[60,61] The phonon dispersion relations of 4-AGNR and 9-AGNR calculated from both DFTB and DFT are compared in the supplementary Fig. S2, showing good agreement, especially for the low frequency phonons (e.g., ω between 0 and 12 THz). Figure 2 displays the calculated phonon dispersion relations of AGNRs for the frequency from 0 to 8 THz (full range phonon dispersion relations are plotted in Fig. S3 along with the phonon dispersion relation of graphene along the high-symmetry path Γ-K). The N-AGNRs are divided into two groups in the plot according to whether N is even or odd. Since the AGNRs are 1D structures, there exist four acoustic phonon modes: longitudinal acoustic (LA),

twisting acoustic (TWA), flexural acoustic (ZA), and transverse acoustic (TA) modes. The ZA and TA phonon branches near Γ point show quadratic dispersion (for graphene, only the ZA phonon branch[39,43]), which leads to zero group velocity as the wavevector approaches Γ point. The TWA phonon branch is unique for 1D materials compared to the 2D materials, which is also observed in other 1D materials.[37,51,62] Also, the phonon branches of AGNRs largely soften compared to graphene, especially for the LA and TA phonon branches. These features demonstrate the size confinement effect when the width is below 1 nm, which is different from the previous study of ZGNRs.[35]

Table 1 The width (W), lattice constant (a), lattice thermal conductivity (κ) at 300 K, and contributions of ZA and total acoustic phonons to κ of the AGNRs. The ratio between a and the corresponding graphene lattice parameter a_0 (a_0 = 4.316 Å) is also listed.

	Width (Å)	a (Å)	κ (W/m-K)	ZA (%)	Acoustic (%)	a/a_0 (%)
4-AGNR	3.464	4.482	3470.6	50.5	93.9	103.85
5-AGNR	4.741	4.433	2137.0	51.3	93.6	102.71
6-AGNR	5.973	4.417	1074.9	49.0	88.7	102.34
7-AGNR	7.231	4.397	884.5	46.6	84.6	101.88
8-AGNR	8.488	4.383	687.5	40.8	75.6	101.55
9-AGNR	9.723	4.379	531.7	35.2	70.3	101.46

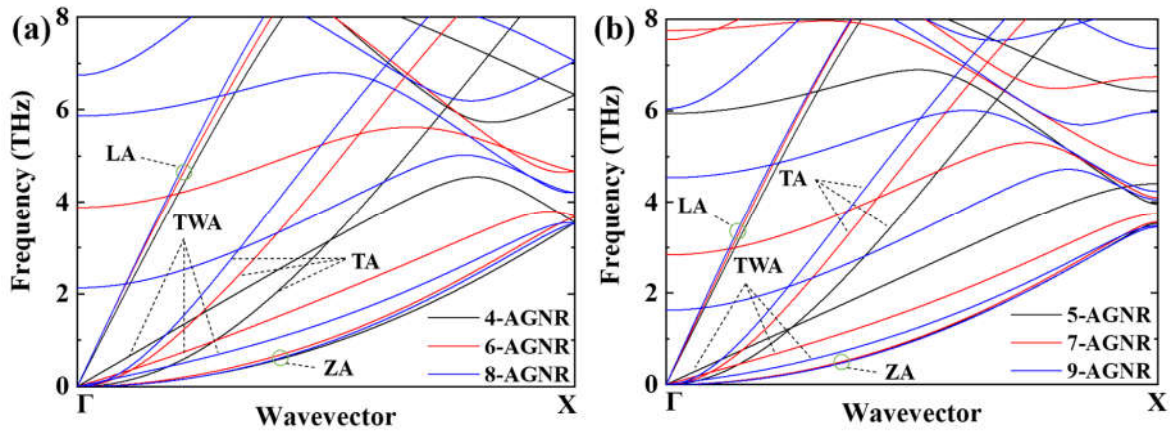

Fig. 2 Phonon dispersion relations of (a) 4-, 6-, and 8-AGNR, and (b) 5-, 7- and 9-AGNR from 0 to 8 THz.

Unlike graphene, in the AGNRs there exist many low frequency optical phonon branches, and the lowest frequency of flexural optical (ZO) phonon modes reaches around 2 THz, smaller than that of most LA and TA phonon modes. Such low frequency optical branches make the acoustic-optical phonon scattering more easily and could reduce the thermal conductivity of AGNRs. However, as the width decreases, the lowest ZO phonon branch of the AGNRs hardens. For instance, the frequency of ZO phonon modes of 9-AGNR at Γ point is below 2 THz, while that of 4-AGNR is around 10 THz, which indicates that the acoustic phonons of AGNRs with smaller width may be less easily scattered by the optical phonons. The phonon group velocity is another key parameter when determining the lattice thermal conductivity. Figure 3 plots the calculated phonon group velocity of the AGNRs and graphene with respect to frequency. It is clear that as the width decreases, the phonon group velocity of low frequency (i.e., $\omega < 4$ THz) phonons increases. Since the low frequency phonons usually carry most of the heat, the width-dependent behavior of their phonon group velocities in AGNRs can strongly affect the lattice thermal conductivity.

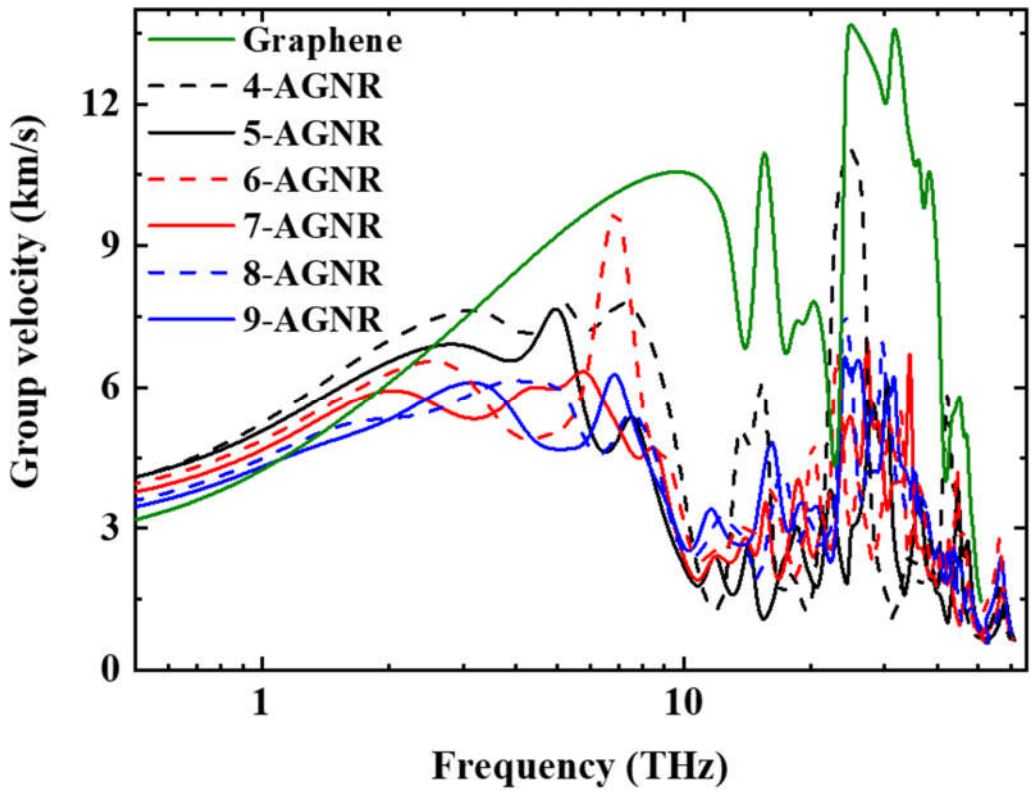

Fig. 3 Phonon group velocity of the AGNRs and graphene.

3.2. Anharmonic properties and lattice thermal conductivity of the AGNRs

The phonon lifetimes of the AGNRs at 300 K are displayed in Fig. 4. It is obvious that the low frequency phonons have longer lifetimes, especially the ZA and TA phonon modes. For the low frequency ZA, TA, and LA phonon modes, their phonon lifetimes increase as the width decreases. The only exception is the TWA phonon branch, whose low frequency phonon lifetimes decrease as the width decreases. However, the lifetimes of the low frequency ZA and TA phonon modes are much larger than those of the low frequency TWA phonon modes. Therefore, the low frequency ZA and TA phonon modes dominate the thermal transport in the AGNRs, and their properties largely influence the width dependence of the lattice thermal conductivity. It is also noted that for small wavevector, the phonon lifetimes of the ZA and TA modes show q^2 dependence, while these of the TWA and LA phonon modes

approach constant (i.e., q independence). Similar q^2 dependence (or q independence) was also observed for the ZA phonon modes (or LA and TA phonon modes) for small wavevector in graphene[43,52,63] and the polyethylene chain.[51]

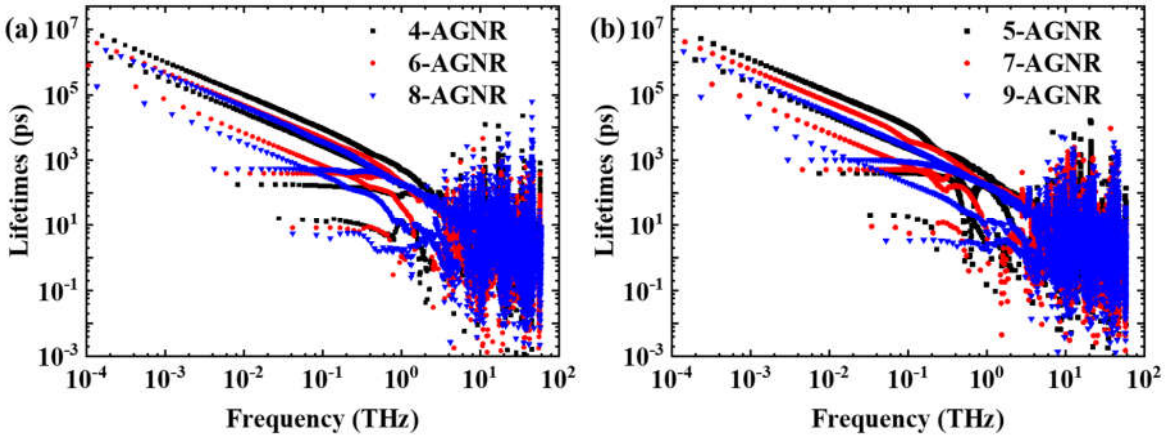

Fig. 4 Phonon lifetimes of (a)4-, 6-, and 8-AGNR, and (b) 5-, 7- and 9-AGNR.

After obtaining the phonon harmonic properties and the lifetimes, the lattice thermal conductivity can be calculated. Our DFTB lattice thermal conductivity of graphene is 4625 W/m-K by considering only three-phonon scattering, which agrees well with previous studies.[43,44,64] It was argued in a few studies based on empirical potentials that four-phonon scattering may contribute to the thermal transport in graphene, despite of lacking first-principles confirmation.[21,65] Figure 5 plots the lattice thermal conductivity of AGNRs with respect to the width at 300 K. As the width decreases from 0.97 to 0.35 nm, the lattice thermal conductivity at 300 K shows a large increase from 532 W/m-K to 3471 W/m-K. At the width of 0.97 nm, the ratio $\kappa_{AGNR}/\kappa_{graphene}$ is around 0.12 according to our DFTB results. With the same ribbon width, the BTE study using a reoptimized empirical potential predicted the ratio $\kappa_{AGNR}/\kappa_{graphene}$ to be 1.05,[37] much larger than our result. Such discrepancy may attribute to the unresolved AGNR structures[35] and the usage of empirical potential in the previous BTE calculation. Other studies involving ultra-narrow AGNRs mostly focused on the phonon ballistic transport regime

(that is, the length of AGNRs is very short),[31,48] which is different from the current work. In Table 1, the absolute values of lattice thermal conductivity and contributions from the ZA and acoustic phonon modes in N-AGNRs are summarized. The acoustic phonon modes dominate the thermal transport in the AGNRs, especially the ZA phonon modes. The ZA and total acoustic phonon contributions also show ascending trends as the width decreases. In 4-AGNR, the low frequency acoustic phonons own the largest group velocities and lifetimes (that is, the longest MFPs), resulting in the highest lattice thermal conductivity. To better understand this, the normalized cumulative thermal conductivity of the AGNRs with respect to the MFP is plotted in Fig. 6. The MFPs corresponding to the 50% contribution of 4-AGNR and 9-AGNR are around 2350 nm and 390 nm, respectively, which implies that phonons with long MFPs contribute more to the thermal transport in the narrower AGNRs. Another 1D material, SWCNT, also shows a similar diameter dependence of thermal conductivity, as demonstrated in both empirical potential[37] and *ab initio* studies.[66] Large enhancement in phonon lifetimes of small-diameter SWCNTs was also reported.[66]

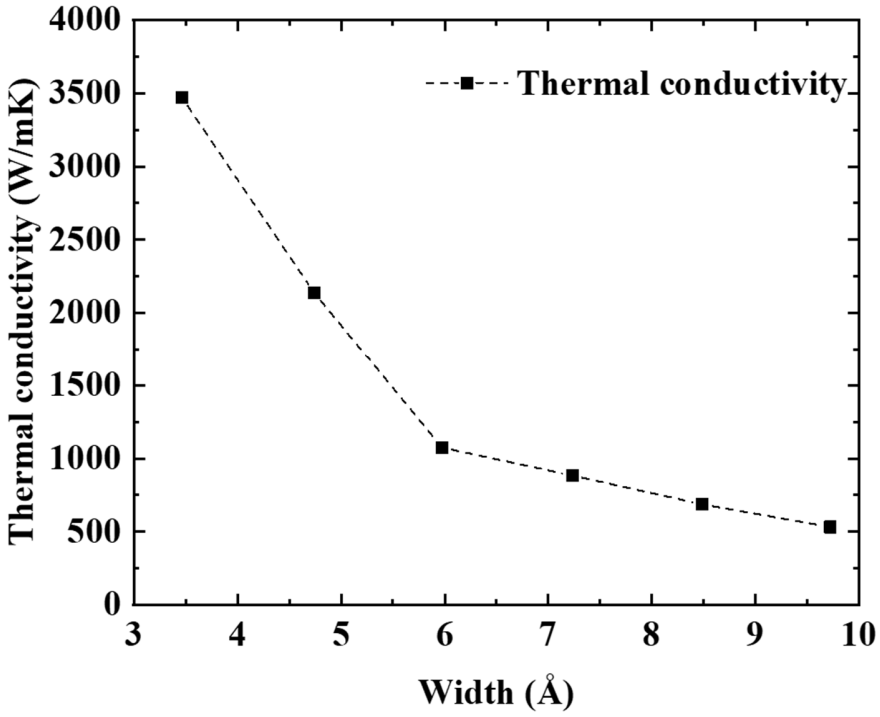

Fig. 5 The lattice thermal conductivity of AGNRs at 300 K.

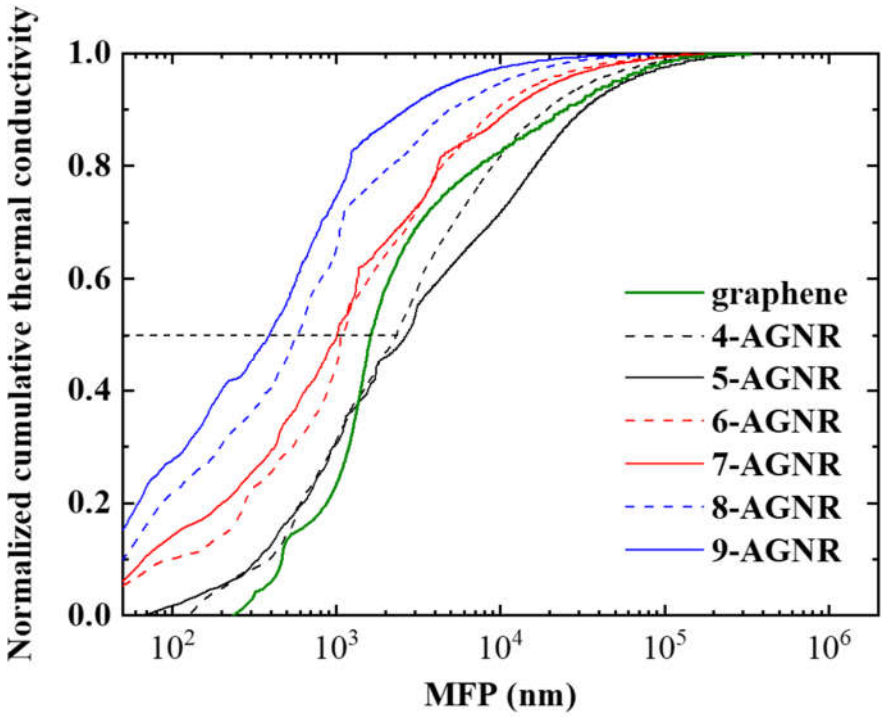

Fig. 6 The normalized cumulative thermal conductivity with respect to the phonon MFP of AGNRs and graphene at 300 K. Only three-phonon scattering is considered. The horizontal dash line denotes the 50% contribution.

To better understand the width-dependent thermal transport, the ratios between the lattice constants of the AGNRs and the corresponding lattice parameter of graphene (a/a_0) are also listed in Table 1. Compared to graphene, the ultra-narrow AGNRs seem to be all elongated slightly (< 4%) along the armchair direction. As the width decreases, the elongation effect is enhanced. To investigate the influence of elongation, the phonon dispersion relations of unstrained 9-AGNR and 9-AGNR with a small tensile strain are displayed in Fig. 7(a). The small tensile strain is set to $(a_{4-AGNR} - a_{9-AGNR})/a_{9-AGNR}$, so that the lattice constant of the strained 9-AGNR is the same as that of 4-AGNR. Compared to unstrained 9-AGNR, the ZA and TWA phonon branches (also the TA phonon

modes near Γ point) of the strained 9-AGNR harden, and the phonon group velocities increase. Previous studies of graphene also demonstrated that small biaxial tensile strain can induce phonon hardening and increase the phonon group velocity, leading to the increase of lattice thermal conductivity.[44,52] Such thermal conductance enhancement induced by small tensile strain is also observed in other 2D materials.[67-69] However, directly applying tensile strain also modifies the acoustic phonon dispersion relations of 9-AGNR near Γ point (e.g., the quadratic ZA dispersion relation near Γ point becomes more linear), and a portion of the low frequency phonon lifetimes (e.g., phonons below 0.3 THz) decrease under tensile strain as shown in Fig. 7(b). It is also noticed that the lowest ZO phonon branch near Γ point is barely influenced by the small tensile strain. Since the gaps between the low frequency ZO phonon modes and ZA or TWA phonon modes near Γ point in the strained 9-AGNR become narrower, the low frequency acoustic-optical phonon scatterings near Γ point may be enhanced under a small tensile strain, leading to the decreased low frequency phonon lifetimes. Thus, the elongation effect mainly hardens the acoustic phonon branches, increases the low frequency phonon group velocities and a portion of low frequency phonon lifetimes. As the width decreases, the elongation effect of the ultra-narrow AGNRs strengthens, and the low frequency phonon group velocities decrease.

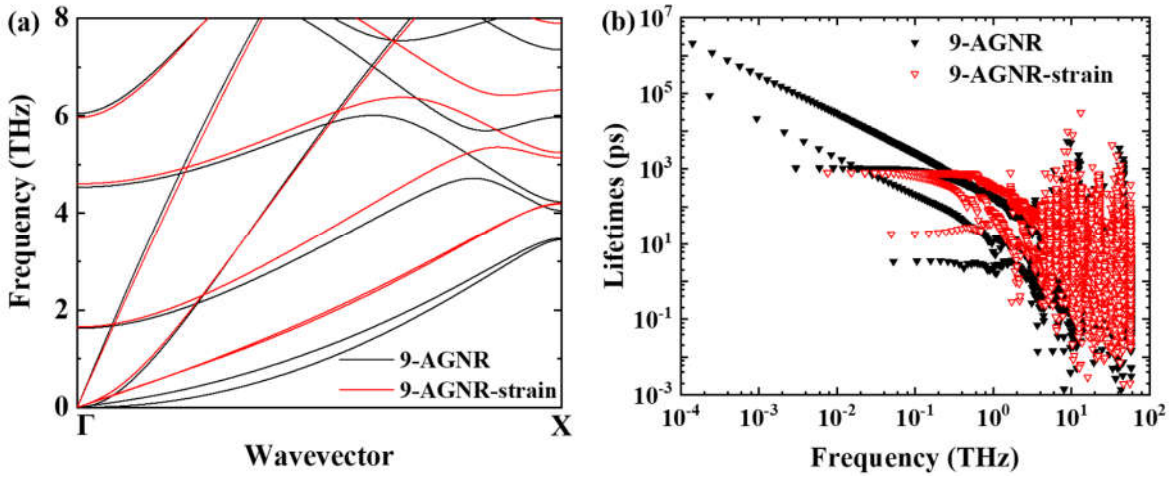

Fig. 7 Phonon (a) dispersion relations and (b) lifetimes of unstrained and strained 9-AGNR. The lattice constant of the strained 9-AGNR is equal to that of 4-AGNR. The thermal conductivity of 9-AGNR increases from 531.7 to 1296.7 W/m-K at 300 K when the tensile strain is applied.

The three-phonon scattering rates are directly related to the phonon scattering channels. The weighted phase space quantifies the three-phonon scattering processes allowed by both energy and momentum conservations.[70,71] A larger weighted phase space suggests more three-phonon scattering channels and shorter phonon lifetimes. Figure 8 plots the calculated weighted phase space of the low frequency phonons in the ultra-narrow AGNRs and graphene. The ultra-narrow AGNRs have significantly more scattering channels than graphene. Also, the low frequency phonons in the narrower AGNRs own fewer phonon scattering channels and consequently, longer phonon lifetimes. As the width decreases, the low frequency ZO branch hardens, and the low frequency acoustic-optical branch gap enlarges, leading to the decrease of phonon scattering channels and increase of phonon lifetimes.

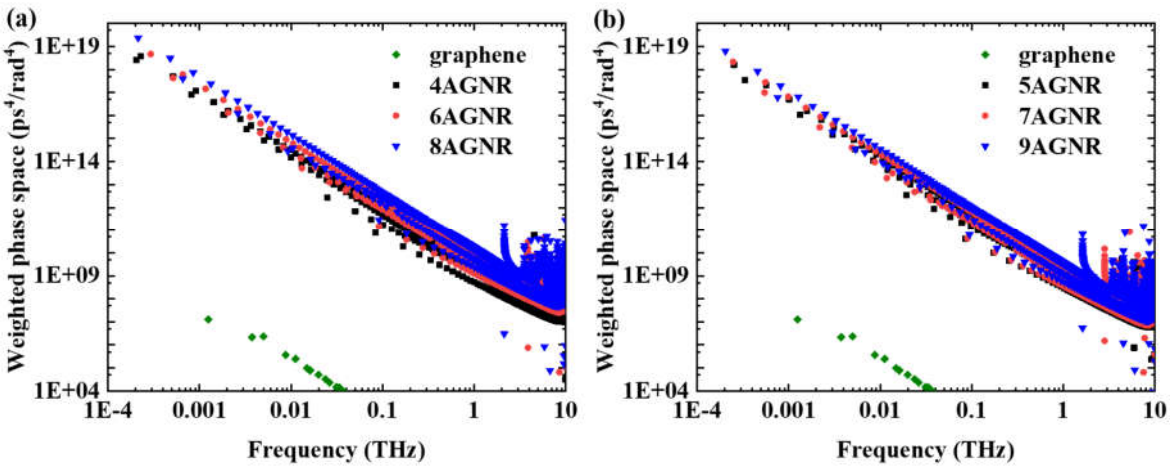

Fig. 8 Weighted phase space *vs* frequency for the ultra-narrow AGNRs and graphene.

Therefore, as the width of the ultra-narrow AGNRs decreases, the enhanced elongation effect of lattice constant increases the low frequency acoustic phonon group velocities and a portion of low

frequency phonon lifetimes, and the decrease of phonon scattering channels of low frequency phonons also induces ascending phonon lifetimes, which together result in an increase of the lattice thermal conductivity. It is expected that the effects of lattice elongation and phonon scattering channels of low frequency phonons will reach saturation as the width increases in larger scales (larger than the width considered here), and the lattice thermal conductivity will reach a minimum value. Meanwhile, the contribution of acoustic phonons keeps decreasing, and the intermediate frequency phonons become more important in thermal transport. Marepalli *et al.* reported that phonon branches of GNRs start grouping together at larger widths, leading to degenerate phonon modes and reduced phonon scattering channels,[35] which account for the ascending thermal conductivity as width increases in the range of larger width. When the width becomes even larger, AGNRs no longer have strict 1D structures, and the acoustic phonon branches will approach those of graphene (e.g., the TA branch near Γ point will change from quadratic to a linear relation). The thermal transport mechanism for the ultra-narrow AGNRs is no longer applicable, and eventually, the lattice thermal conductivity of AGNRs will approach to the bulk value of graphene. It is also worth mentioning that the edges of ultra-narrow AGNRs in this study are well-defined and are possibly the smoothest; in other words, edge scattering is neglected, which is different from the traditional macroscale models. In the macroscale regime, the edge or surface roughness is always considered classically, which plays a significant role in suppressing thermal transport as the size decreases because of the increasing surface/volume or edge/plane ratio.[46]

3.3. Thermal transport in ABNNRs

After exploring the width dependence of thermal conductivity of the ultra-narrow AGNRs, a question naturally arises: does this behavior occur in other similar quasi-1D materials? The planar monolayer h-BN shares a similar honeycomb structure with graphene and has relatively high thermal conductivity.[43,72,73] The phonon dispersion relation of the ZA branch is also quadratic near Γ point.[43,73]

To address the above question, the thermal properties of N-ABNNRs (N: 5-10) are investigated at 300 K. The lattice thermal conductivity of monolayer *h*-BN is predicted to be 1140 W/m-K based on our DFTB calculations taking into account the three-phonon scattering, which agrees well with the first-principles calculations.[74] Analogously, with small biaxial tensile strain, the lattice thermal conductivity of monolayer *h*-BN was predicted to increase.[69,75] The optimized structures of ultra-narrow ABNNRs are shown in Fig. S4. Compared to the AGNRs, although the edges of ABNNRs undergo minor reconstruction, they are still well-defined. Such reconstruction does not affect the phonon dispersion relations and lifetimes, as demonstrated in Fig. 9. The structural parameters, lattice thermal conductivity at 300 K, contributions of the ZA and total acoustic phonons are listed in Table 2. As the width decreases, the lattice thermal conductivity of the ultra-narrow ABNNRs increases, which is consistent with the trend for the ultra-narrow AGNRs. Comparing to the ultra-narrow AGNRs, similar width-dependent relations of other structural parameters (a, a/a_0) and thermal properties (phonon group velocity, lifetimes) are also observed in the ultra-narrow ABNNRs, providing further supports for our analysis and conclusion. The width dependence of the ultra-narrow AGNRs and ABNNRs and the resolved mechanism behind may be extrapolated to other ultra-narrow 1D planar or buckling nanoribbons, providing a deeper insight into the precise thermal management of potential nano electronics.

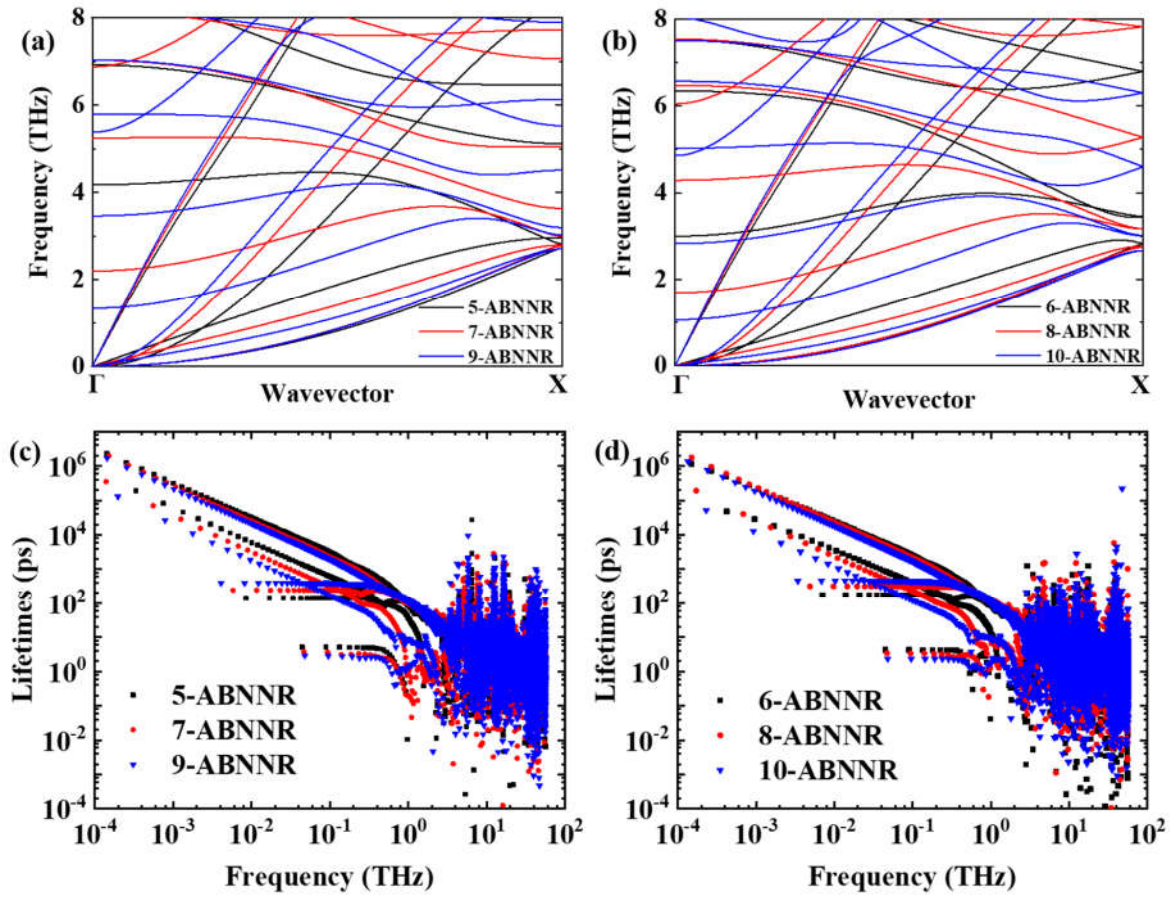

Fig. 9 Phonon (a) dispersion relations and (c) lifetimes of 5-, 7-, and 9-ABNNRs. Phonon (b) dispersion relations and (d) lifetimes of 6-, 8- and 10-ABNNRs.

Table 2 The width (W), lattice constant (a), lattice thermal conductivity (κ) at 300 K, and contributions of ZA and total acoustic phonons to the lattice thermal conductivity of ABNNRs. The ratio between a and the corresponding 2D h-BN lattice parameter a_0 (a_0 = 4.416 Å) is also listed.

	Width (Å)	a (Å)	κ (W/m-K)	ZA (%)	Acoustic (%)	a/a_0 (%)
5-ABNNR	5.180	4.487	567.5	51.06	93.3	101.61

6-ABNNR	6.484	4.468	411.9	46.72	87.79	101.18
7-ABNNR	7.750	4.460	357.5	44.17	84.58	101.00
8-ABNNR	9.036	4.452	322.8	40.71	80.08	100.81
9-ABNNR	10.310	4.448	271.7	36.73	74.17	100.72
10-ABNNR	11.589	4.444	242.8	33.67	70.92	100.63

4. Conclusions

In summary, based on DFTB calculations within the BTE scheme, we have predicted the thermal properties of the ultra-narrow AGNRs without hydrogen termination at 300 K and extracted their width dependence. The lattice thermal conductivity of the ultra-narrow AGNRs increases from 531.7 W/m-K to 3470.6 W/m-K as the width decreases from 0.97 to 0.35 nm at 300 K, which is attributed to the behavior of the dominant low frequency acoustic phonons. Accordingly, the lattice constants, low frequency phonon group velocities and lifetimes, and acoustic phonon contributions also show increasing trends. As the width decreases, the elongation of lattice constant along the armchair direction enhances, and the number of phonon scattering channels of low frequency acoustic phonons decreases, leading to the increase of the low frequency acoustic phonon group velocities and lifetimes, and consequently, the lattice thermal conductivity. Additionally, planar ultra-narrow ABNNRs show analogous trends in thermal properties with respect to the width, which provides further supports for our analysis. This work provides a fundamental physical understanding of thermal transport in nanoribbons and may benefit the thermal design of atomically precise nano electronics.

Acknowledgments

This work is supported by the National Natural Science Foundation of China (51706192 and 11874313), the Research Grants Council of Hong Kong (17300018 and 17201019), and the Zhejiang Provincial Natural Science Foundation (LR19A040001). The authors are grateful for the research computing facilities offered by ITS, HKU.

Supporting Information

Convergence test results of the lattice thermal conductivity of the ultra-narrow AGNRs; electronic band structures of AGNRs with different widths; phonon dispersion relations of 4-AGNR and 9-AGNR calculated from DFTB and DFT; phonon dispersion relations of the ultra-narrow AGNRs and graphene in full frequency range; optimized structures of 5-ABNNR and 6-ABNNR.

Reference

1. Papageorgiou, D. G.; Kinloch, I. A.; Young, R. J., Mechanical properties of graphene and graphene-based nanocomposites. *Prog. Mater. Sci.* **2017,** *90*, 75-127.
2. Sang, M.; Shin, J.; Kim, K.; Yu, K. J., Electronic and thermal properties of graphene and recent advances in graphene based electronics applications. *Nanomaterials* **2019,** *9* (3), 374.
3. Yan, Z.; Nika, D. L.; Balandin, A. A., Thermal properties of graphene and few-layer graphene: Applications in electronics. *IET Circuits, Devices Syst.* **2015,** *9* (1), 4-12.
4. Son, Y. W.; Cohen, M. L.; Louie, S. G., Energy gaps in graphene nanoribbons. *Phys. Rev. Lett.* **2006,** *97* (21), 216803.
5. Chen, Y. C.; de Oteyza, D. G.; Pedramrazi, Z.; Chen, C.; Fischer, F. R.; Crommie, M. F., Tuning the band gap of graphene nanoribbons synthesized from molecular precursors. *ACS Nano* **2013,** *7* (7), 6123-6128.
6. Barone, V.; Hod, O.; Scuseria, G. E., Electronic structure and stability of semiconducting graphene nanoribbons. *Nano Lett.* **2006,** *6* (12), 2748-2754.
7. Chen, Y. C.; Cao, T.; Chen, C.; Pedramrazi, Z.; Haberer, D.; de Oteyza, D. G.; Fischer, F. R.; Louie, S. G.; Crommie, M. F., Molecular bandgap engineering of bottom-up synthesized graphene nanoribbon heterojunctions. *Nat. Nanotechnol.* **2015,** *10* (2), 156-160.
8. Li, X.; Zhang, T. Y.; Su, Y. J., Periodically modulated size-dependent elastic properties of armchair graphene nanoribbons. *Nano Lett.* **2015,** *15* (8), 4883-4888.
9. Zhao, H.; Min, K.; Aluru, N. R., Size and chirality dependent elastic properties of graphene nanoribbons under uniaxial tension. *Nano Lett.* **2009,** *9* (8), 3012-3015.
10. Chu, Y.; Ragab, T.; Basaran, C., The size effect in mechanical properties of finite-sized graphene nanoribbon. *Comput. Mater. Sci.* **2014,** *81*, 269-274.
11. Son, Y. W.; Cohen, M. L.; Louie, S. G., Half-metallic graphene nanoribbons. *Nature* **2006,** *444* (7117), 347-349.
12. Kan, M.; Zhou, J.; Sun, Q.; Wang, Q.; Kawazoe, Y.; Jena, P., Tuning magnetic properties of graphene nanoribbons with topological line defects: From antiferromagnetic to ferromagnetic. *Phys. Rev. B* **2012,** *85* (15), 155450.
13. Cao, T.; Zhao, F.; Louie, S. G., Topological phases in graphene nanoribbons: Junction states, spin centers, and quantum spin chains. *Phys. Rev. Lett.* **2017,** *119* (7), 076401.
14. Rizzo, D. J.; Veber, G.; Cao, T.; Bronner, C.; Chen, T.; Zhao, F.; Rodriguez, H.; Louie, S. G.; Crommie, M. F.; Fischer, F. R., Topological band engineering of graphene nanoribbons. *Nature* **2018,** *560* (7717), 204-208.
15. Groning, O.; Wang, S.; Yao, X.; Pignedoli, C. A.; Borin Barin, G.; Daniels, C.; Cupo, A.; Meunier, V.; Feng, X.; Narita, A.; Mullen, K.; Ruffieux, P.; Fasel, R., Engineering of robust topological quantum phases in graphene nanoribbons. *Nature* **2018,** *560* (7717), 209-213.
16. Bae, M.-H.; Li, Z.; Aksamija, Z.; Martin, P. N.; Xiong, F.; Ong, Z.-Y.; Knezevic, I.; Pop, E., Ballistic to diffusive crossover of heat flow in graphene ribbons. *Nat. Commun.* **2013,** *4* (1), 1734.
17. Xu, X.; Pereira, L. F. C.; Wang, Y.; Wu, J.; Zhang, K.; Zhao, X.; Bae, S.; Tinh Bui, C.; Xie, R.; Thong, J. T. L.; Hong, B. H.; Loh, K. P.; Donadio, D.; Li, B.; Özyilmaz, B., Length-dependent thermal conductivity in suspended single-layer graphene. *Nat. Commun.* **2014,** *5* (1), 3689.
18. Wang, H.; Kurata, K.; Fukunaga, T.; Zhang, X.; Takamatsu, H., Width dependent intrinsic thermal conductivity of suspended monolayer graphene. *Int. J. Heat Mass Transfer* **2017,** *105*, 76-80.
19. Chen, L.; Xie, H.; Yu, W.; Wang, B.; Wu, Z., Thermal transport behaviors of suspended graphene sheets with different sizes. *Int. J. Therm. Sci.* **2015,** *94*, 221-227.

20. Chen, S.; Moore, A. L.; Cai, W.; Suk, J. W.; An, J.; Mishra, C.; Amos, C.; Magnuson, C. W.; Kang, J.; Shi, L.; Ruoff, R. S., Raman measurements of thermal transport in suspended monolayer graphene of variable sizes in vacuum and gaseous environments. *ACS Nano* **2011,** *5* (1), 321-328.
21. Feng, T.; Ruan, X., Four-phonon scattering reduces intrinsic thermal conductivity of graphene and the contributions from flexural phonons. *Phys. Rev. B* **2018,** *97* (4), 045202.
22. Vallabhaneni, A. K.; Singh, D.; Bao, H.; Murthy, J.; Ruan, X., Reliability of Raman measurements of thermal conductivity of single-layer graphene due to selective electron-phonon coupling: A first-principles study. *Phys. Rev. B* **2016,** *93* (12), 125432.
23. Li, Q.-Y.; Feng, T.; Okita, W.; Komori, Y.; Suzuki, H.; Kato, T.; Kaneko, T.; Ikuta, T.; Ruan, X.; Takahashi, K., Enhanced thermoelectric performance of as-grown suspended graphene nanoribbons. *ACS Nano* **2019,** *13* (8), 9182-9189.
24. Murali, R.; Yang, Y.; Brenner, K.; Beck, T.; Meindl, J. D., Breakdown current density of graphene nanoribbons. *Appl. Phys. Lett.* **2009,** *94* (24), 243114.
25. Nguyen, G. D.; Tsai, H.-Z.; Omrani, A. A.; Marangoni, T.; Wu, M.; Rizzo, D. J.; Rodgers, G. F.; Cloke, R. R.; Durr, R. A.; Sakai, Y.; Liou, F.; Aikawa, A. S.; Chelikowsky, J. R.; Louie, S. G.; Fischer, F. R.; Crommie, M. F., Atomically precise graphene nanoribbon heterojunctions from a single molecular precursor. *Nat. Nanotechnol.* **2017,** *12* (11), 1077-1082.
26. Talirz, L.; Ruffieux, P.; Fasel, R., On-surface synthesis of atomically precise graphene nanoribbons. *Adv. Mater.* **2016,** *28* (29), 6222-6231.
27. Haskins, J.; Kınacı, A.; Sevik, C.; Sevinçli, H.; Cuniberti, G.; Çağın, T., Control of thermal and electronic transport in defect-engineered graphene nanoribbons. *ACS Nano* **2011,** *5* (5), 3779-3787.
28. Guo, Z.; Zhang, D.; Gong, X.-G., Thermal conductivity of graphene nanoribbons. *Appl. Phys. Lett.* **2009,** *95* (16), 163103.
29. Hu, J.; Ruan, X.; Chen, Y. P., Thermal conductivity and thermal rectification in graphene nanoribbons: A molecular dynamics study. *Nano Lett.* **2009,** *9* (7), 2730-2735.
30. Ye, Z.-Q.; Cao, B.-Y.; Yao, W.-J.; Feng, T.; Ruan, X., Spectral phonon thermal properties in graphene nanoribbons. *Carbon* **2015,** *93*, 915-923.
31. Xu, Y.; Chen, X.; Gu, B.-L.; Duan, W., Intrinsic anisotropy of thermal conductance in graphene nanoribbons. *Appl. Phys. Lett.* **2009,** *95* (23), 233116.
32. Evans, W. J.; Hu, L.; Keblinski, P., Thermal conductivity of graphene ribbons from equilibrium molecular dynamics: Effect of ribbon width, edge roughness, and hydrogen termination. *Appl. Phys. Lett.* **2010,** *96* (20), 203112.
33. Wang, Y.; Qiu, B.; Ruan, X., Edge effect on thermal transport in graphene nanoribbons: A phonon localization mechanism beyond edge roughness scattering. *Appl. Phys. Lett.* **2012,** *101* (1), 013101.
34. Ma, D.; Wan, X.; Yang, N., Unexpected thermal conductivity enhancement in pillared graphene nanoribbon with isotopic resonance. *Phys. Rev. B* **2018,** *98* (24), 245420.
35. Marepalli, P.; Singh, D.; Murthy, J. Y., Spectrally-resolved thermal transport in graphene nanoribbons. *J. Appl. Phys.* **2019,** *125* (23), 234302.
36. Lindsay, L.; Broido, D. A., Optimized Tersoff and Brenner empirical potential parameters for lattice dynamics and phonon thermal transport in carbon nanotubes and graphene. *Phys. Rev. B* **2010,** *81* (20), 205441.
37. Lindsay, L.; Broido, D. A.; Mingo, N., Diameter dependence of carbon nanotube thermal conductivity and extension to the graphene limit. *Phys. Rev. B* **2010,** *82* (16), 161402.
38. Brenner, D. W., Empirical potential for hydrocarbons for use in simulating the chemical vapor deposition of diamond films. *Phys. Rev. B* **1990,** *42* (15), 9458-9471.

39. Lindsay, L.; Broido, D. A.; Mingo, N., Flexural phonons and thermal transport in graphene. *Phys. Rev. B* **2010,** *82* (11), 115427.
40. Broido, D. A.; Malorny, M.; Birner, G.; Mingo, N.; Stewart, D. A., Intrinsic lattice thermal conductivity of semiconductors from first principles. *Appl. Phys. Lett.* **2007,** *91* (23), 231922.
41. Lindsay, L.; Hua, C.; Ruan, X. L.; Lee, S., Survey of ab initio phonon thermal transport. *Mater. Today Phys.* **2018,** *7*, 106-120.
42. Li, S.; Ma, J.; Pei, Y.; Chen, Y., Anharmonic lattice dynamics of Te and its counter-intuitive strain dependent lattice thermal conductivity. *J. Mater. Chem. C* **2019,** *7* (20), 5970-5974.
43. Kuang, Y.; Lindsay, L.; Huang, B., Unusual enhancement in intrinsic thermal conductivity of multilayer graphene by tensile strains. *Nano Lett.* **2015,** *15* (9), 6121-6127.
44. Kuang, Y.; Lindsay, L.; Shi, S.; Wang, X.; Huang, B., Thermal conductivity of graphene mediated by strain and size. *Int. J. Heat Mass Transfer* **2016,** *101*, 772-778.
45. Wang, X.; Guo, R.; Xu, D.; Chung, J.; Kaviany, M.; Huang, B., Anisotropic lattice thermal conductivity and suppressed acoustic phonons in MOF-74 from first principles. *J. Phys. Chem. C* **2015,** *119* (46), 26000-26008.
46. Wang, Q.; Guo, R.; Chi, C.; Zhang, K.; Huang, B., Direct first-principle-based study of mode-wise in-plane phonon transport in ultrathin silicon films. *Int. J. Heat Mass Transfer* **2019,** *143*, 118507.
47. Wang, Q.; Wang, X.; Guo, R.; Huang, B., Parametrization of density functional tight-binding method for thermal transport in bulk and low-dimensional Si systems. *J. Phys. Chem. C* **2017,** *121* (28), 15472-15480.
48. Tan, Z. W.; Wang, J.-S.; Gan, C. K., First-principles study of heat transport properties of graphene nanoribbons. *Nano Lett.* **2011,** *11* (1), 214-219.
49. MacDonald, A. H.; Vosko, S. H.; Coleridge, P. T., Extensions of the tetrahedron method for evaluating spectral properties of solids. *J. Phys. C: Solid State Phys.* **1979,** *12* (15), 2991-3002.
50. Togo, A.; Chaput, L.; Tanaka, I., Distributions of phonon lifetimes in Brillouin zones. *Phys. Rev. B* **2015,** *91* (9), 094306.
51. Wang, X.; Kaviany, M.; Huang, B., Phonon coupling and transport in individual polyethylene chains: A comparison study with the bulk crystal. *Nanoscale* **2017,** *9* (45), 18022-18031.
52. Bonini, N.; Garg, J.; Marzari, N., Acoustic phonon lifetimes and thermal transport in free-standing and strained graphene. *Nano Lett.* **2012,** *12* (6), 2673-2678.
53. Hourahine, B.; Aradi, B.; Blum, V.; Bonafé, F.; Buccheri, A.; Camacho, C.; Cevallos, C.; Deshaye, M. Y.; Dumitrică, T.; Dominguez, A.; Ehlert, S.; Elstner, M.; Heide, T. v. d.; Hermann, J.; Irle, S.; Kranz, J. J.; Köhler, C.; Kowalczyk, T.; Kubař, T.; Lee, I. S.; Lutsker, V.; Maurer, R. J.; Min, S. K.; Mitchell, I.; Negre, C.; Niehaus, T. A.; Niklasson, A. M. N.; Page, A. J.; Pecchia, A.; Penazzi, G.; Persson, M. P.; Řezáč, J.; Sánchez, C. G.; Sternberg, M.; Stöhr, M.; Stuckenberg, F.; Tkatchenko, A.; Yu, V. W.-z.; Frauenheim, T., DFTB+, a software package for efficient approximate density functional theory based atomistic simulations. *J. Chem. Phys.* **2020,** *152* (12), 124101.
54. Gaus, M.; Goez, A.; Elstner, M., Parametrization and benchmark of DFTB3 for organic molecules. *J. Chem. Theory Comput.* **2013,** *9* (1), 338-354.
55. Lukose, B.; Kuc, A.; Frenzel, J.; Heine, T., On the reticular construction concept of covalent organic frameworks. *Beilstein J. Nanotechnol.* **2010,** *1*, 60-70.
56. Elstner, M.; Porezag, D.; Jungnickel, G.; Elsner, J.; Haugk, M.; Frauenheim, T.; Suhai, S.; Seifert, G., Self-consistent-charge density-functional tight-binding method for simulations of complex materials properties. *Phys. Rev. B* **1998,** *58* (11), 7260-7268.

57. Frauenheim, T.; Seifert, G.; Elsterner, M.; Hajnal, Z.; Jungnickel, G.; Porezag, D.; Suhai, S.; Scholz, R., A self-consistent charge density-functional based tight-binding method for predictive materials simulations in physics, chemistry and biology. *phys. stat. sol. (b)* **2000,** *217* (1), 41-62.
58. Yang; Yu, H.; York, D.; Cui, Q.; Elstner, M., Extension of the self-consistent-charge density-functional tight-binding method: Third-order expansion of the density functional theory total energy and introduction of a modified effective Coulomb interaction. *J. Phys. Chem. A* **2007,** *111* (42), 10861-10873.
59. Elstner, M., The SCC-DFTB method and its application to biological systems. *Theor. Chem. Acc.* **2006,** *116* (1), 316-325.
60. Tabarraei, A.; Shadalou, S.; Song, J.-H., Mechanical properties of graphene nanoribbons with disordered edges. *Comput. Mater. Sci.* **2015,** *96*, 10-19.
61. Gillen, R.; Mohr, M.; Thomsen, C.; Maultzsch, J., Vibrational properties of graphene nanoribbons by first-principles calculations. *Phys. Rev. B* **2009,** *80* (15), 155418.
62. Peelaers, H.; Partoens, B.; Peeters, F. M., Phonon band structure of Si nanowires: A stability analysis. *Nano Lett.* **2009,** *9* (1), 107-111.
63. Lindsay, L.; Li, W.; Carrete, J.; Mingo, N.; Broido, D. A.; Reinecke, T. L., Phonon thermal transport in strained and unstrained graphene from first principles. *Phys. Rev. B* **2014,** *89* (15), 155426.
64. Ma, F.; Zheng, H. B.; Sun, Y. J.; Yang, D.; Xu, K. W.; Chu, P. K., Strain effect on lattice vibration, heat capacity, and thermal conductivity of graphene. *Appl. Phys. Lett.* **2012,** *101* (11), 111904.
65. Gu, X.; Fan, Z.; Bao, H.; Zhao, C. Y., Revisiting phonon-phonon scattering in single-layer graphene. *Phys. Rev. B* **2019,** *100* (6), 064306.
66. Yue, S.-Y.; Ouyang, T.; Hu, M., Diameter dependence of lattice thermal conductivity of single-walled carbon nanotubes: Study from ab initio. *Sci. Rep.* **2015,** *5* (1), 15440.
67. Kuang, Y. D.; Lindsay, L.; Shi, S. Q.; Zheng, G. P., Tensile strains give rise to strong size effects for thermal conductivities of silicene, germanene and stanene. *Nanoscale* **2016,** *8* (6), 3760-3767.
68. Xie, H.; Ouyang, T.; Germaneau, É.; Qin, G.; Hu, M.; Bao, H., Large tunability of lattice thermal conductivity of monolayer silicene via mechanical strain. *Phys. Rev. B* **2016,** *93* (7), 075404.
69. Zhang, Y.-Y.; Pei, Q.-X.; Liu, H.-Y.; Wei, N., Thermal conductivity of a h-BCN monolayer. *Phys. Chem. Chem. Phys.* **2017,** *19* (40), 27326-27331.
70. Li, W.; Mingo, N., Thermal conductivity of fully filled skutterudites: Role of the filler. *Phys. Rev. B* **2014,** *89* (18), 184304.
71. Li, W.; Mingo, N., Ultralow lattice thermal conductivity of the fully filled skutterudite $YbFe_4Sb_{12}$ due to the flat avoided-crossing filler modes. *Phys. Rev. B* **2015,** *91* (14), 6.
72. Cai, Q. R.; Scullion, D.; Gan, W.; Falin, A.; Zhang, S. Y.; Watanabe, K.; Taniguchi, T.; Chen, Y.; Santos, E. J. G.; Li, L. H., High thermal conductivity of high-quality monolayer boron nitride and its thermal expansion. *Sci. Adv.* **2019,** *5* (6).
73. Illera, S.; Pruneda, M.; Colombo, L.; Ordejón, P., Thermal and transport properties of pristine single-layer hexagonal boron nitride: A first principles investigation. *Phys. Rev. Mater.* **2017,** *1* (4), 044006.
74. Cepellotti, A.; Fugallo, G.; Paulatto, L.; Lazzeri, M.; Mauri, F.; Marzari, N., Phonon hydrodynamics in two-dimensional materials. *Nat. Commun.* **2015,** *6* (1), 6400.
75. Li, S.; Chen, Y., Thermal transport and anharmonic phonons in strained monolayer hexagonal boron nitride. *Sci. Rep.* **2017,** *7* (1), 43956.